

LOCAL DISCRIMINATIVE CHARACTERIZATION OF MRI FOR ALZHEIMER'S DISEASE

Ahmad Chaddad, Christian Desrosiers, Matthew Toews

Laboratory for Imagery, Vision and Artificial Intelligence
École de technologie supérieure,
Montreal, Canada, H3C 1K3

ABSTRACT

A novel method is proposed for characterizing Alzheimer's disease (AD) in brain MRI using local image texture features. Texture features are computed from local sub-volumes of T1-weighted MR images, and automatic classification performance is used to identify the (brain region, texture feature) combinations that are most discriminative regarding subject groups, i.e. AD vs healthy subjects. Experiments include MRI data of 124 subjects from the public OASIS database, three commonly-used texture feature types including the 3D-GLCM, 3D-DWT and LoG filters and random forest classification. The method identifies numerous (brain region, texture feature) combinations leading to high classification accuracy ($> 70\%$), including several regions not traditionally linked to AD. These may indicate novel computational biomarkers for computer-assisted diagnosis or characterization of AD. The approach is generally applicable to other 3D data and disease contexts.

Index Terms— Alzheimer's disease, MRI, brain, texture feature, GLCM, LoG, DWT, classification, random forests

1. INTRODUCTION

Alzheimer's disease (AD) is a debilitating, terminal illness closely linked to aging, with symptoms including memory loss, orientation problems, poor judgment, inability to carry out routine tasks, and withdrawal from social activities [1]. It is also a major public health concern, particularly in developed nations with aging populations, as the probability of developing AD is estimated to double every five years after the age of 60 [2]. In this context, there is a critical need for non-invasive methods based on brain imaging to facilitate the characterization, diagnosis and treatment of AD.

Over the years, various methods have been proposed for the automated detection and analysis of AD from brain imaging data. In most of these methods, neuroanatomical biomarkers are used to describe physiological properties of AD-affected brain regions such as the hippocampus and entorhinal cortex [3]. Advanced stages of AD are characterized by more prominent changes to the brain, often in the form of cortical atrophy and the enlargement of ventricles (see

Fig. 1). In [4], an automated segmentation model was used to extract biomarkers representing the volume and tissue thickness of prominent brain regions. This study showed that the entorhinal cortex thickness, hippocampal volume, and supramarginal gyrus thickness could be used to identify mild cognitive impairments (MCI) and AD. In [5], measures of brain tissue volume and hippocampus size were used in combination with an ensemble of classifiers for the early diagnosis of AD, achieving an accuracy of 93.75%. More complex morphological features have also been proposed for the study of AD. In [6], hippocampal shape features based on spherical harmonics were used with an SVM classifier to detect subjects suffering from AD. Another morphometry approach, based on 3D SIFT features and Bayesian classification, was proposed in [7]. A significant advantage of this approach is that it does not require brain volumes to be registered, nor the segmentation of regions of interest.

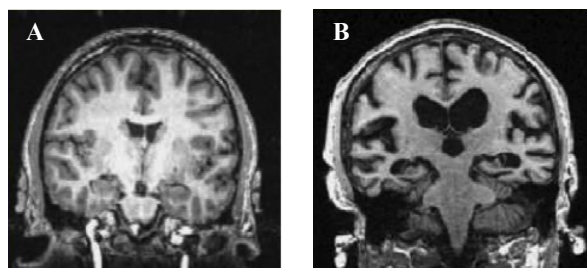


Fig. 1. Coronal T1-weighted MRI scans of NC (A) and patient with AD (B). Hallmark neuroanatomical signs of AD include cortical atrophy, particularly in the mid-temporal regions, and enlargement of extra-cerebral cavities including ventricles.

Neuroanatomical tissue variations due to AD are still not fully understood. Texture features computed from neuroimaging data can potentially help by quantifying the heterogeneity of brain tissues in subjects suffering from this disease [8]. In [9], texture features based on histogram moments, gray-level co-occurrence matrices (GLCM) and discrete wavelets were used to characterize the hippocampal region of AD subjects. Likewise, a method using 3D discrete wavelets was proposed in [10] to differentiate between AD

and control subjects, based on five regions of interest: hippocampus, amygdala, lateral ventricles, anterior cingulate, and posterior cingulate. Finally, gray-level invariant features based on Local Binary Patterns (LBP) have also been proposed to identify elderly subjects suffering from AD using multicenter MRI data [11].

Most studies on the automated detection and characterization of AD from MRI data have focused on well-known regions of interest such as the hippocampus. Although this leads to high detection rates, it does not capture the full spectrum of brain changes related to AD. Recently, a voxel-based analysis using 3D GLCM features (auto-correlation, dissimilarity, variance, sum average and sum entropy) was proposed to characterize whole brain textural differences between AD and control subjects [12]. This analysis revealed significant regional differences between texture features computed throughout the brain, e.g. within the corpus callosum, the temporal lobe, etc. Furthermore, was shown that dissimilarities occurring in different brain regions are related to different GLCM features.

In this paper, we extend the analysis of [12] by investigating three different texture feature types, including the 3D GLCM, the Laplacian of Gaussian (LoG) filter and the 3D discrete wavelet transform (DWT) filter. We use this multi-textural information to determine discriminative brain regions in a data-driven manner, without having to segment specific ROIs. Our results show the usefulness of different texture features in characterizing distinct brain regions affected by AD. Another contribution of our work is to identify texture-based biomarkers in regions not traditionally linked to AD, that may potentially help to better understand and characterize the disease.

2. MATERIALS AND METHODS

2.1. Subject population and data acquisition

Experiments use the publicly available Open Access Series of Imaging Studies (OASIS) database [13], including structural T1-weighted MP-RAGE (Magnetization-Prepared Rapid-Acquisition Gradient Echo) images acquired on a 1.5T Vision scanner in a single imaging session, processed at 1mm isotropic resolution. All image data are spatially aligned via a 3D affine transform, thus establishing region-to-region correspondence across subjects. From this database, we selected all subjects with known clinical dementia rating (CDR), 62 diagnosed as AD (very mild dementia, CDR=0.5) and 62 diagnosed healthy elderly controls/normal (CDR=0). The demographic information and mini-mental state examination (MMSE) score of selected subjects are given in Table 1.

2.2. Proposed method

The outline of the proposed method is shown in Fig. 2. For LoG and 3D-DWT texture features, the corresponding 3D fil-

Table 1. Demographics and mean test scores for Alzheimer’s (AD) and control (NC) subjects.

	AD	NC
Nb of subjects	62	62
Female/Male	36/26	45/17
Age (mean \pm stdev)	75.67 \pm 10.13	70.06 \pm 13.85
MMSE (mean \pm stdev)	25.53 \pm 3.60	29.19 \pm 1.11

ter is first applied on the volumetric metric data. The filtered 3D image is then split using a $10 \times 10 \times 10$ grid, resulting into sub-volumes of $21 \times 18 \times 18$ voxels. The texture in each sub-volume is encoded into a set of features by applying specific quantifier functions. In contrast, 3D-GLCM texture features are computed directly in the sub-volumes, without applying a filter. The three types of texture features are used to train random forest models for classifying subjects as AD or control. Discriminative sub-volumes are selected as those having an accuracy greater than 70% for a given texture type. Details of the proposed method are given in the following sub-sections.

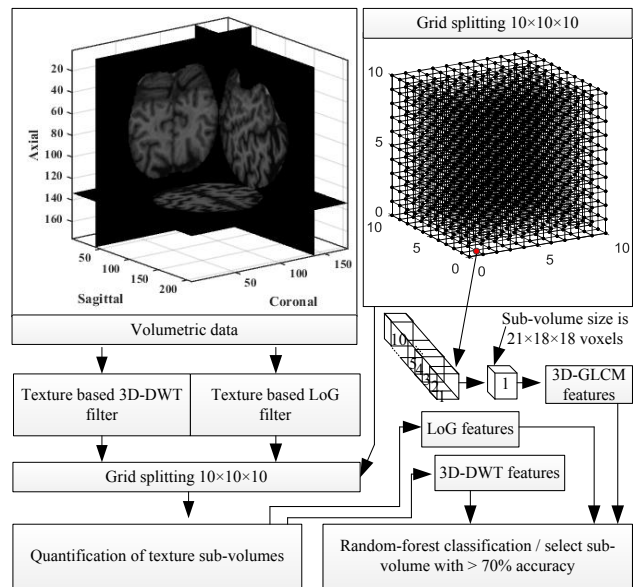


Fig. 2. Outline of the proposed method.

2.2.1. 3D-GLCM

Gray-level co-occurrence matrix (GLCM) features are popular second order statistics that estimate the properties of two or more pixel values occurring at specific locations relative to each other [14]. In this work, we divided each 3D volume using a $10 \times 10 \times 10$ grid, and computed the 3D-GLCM texture features of each sub-volume. Discretizing the intensity values into 8 gray levels, for each sub-volume, we obtained 13 matrices of size 8×8 , each one containing the number of pixel pairs having a given combination of gray levels and a specific

relative position (single offset of 1 pixel, 13 directions).

Each matrix was then encoded using 12 quantifier functions corresponding to energy, entropy, correlation, contrast, homogeneity, variance, sum-mean inertia, cluster-shade, cluster-tendency, maximum probability and inverse variance. Using this strategy, a total of 156 texture features was generated for each sub-volume.

2.2.2. LoG filter

A Laplacian of Gaussian (LoG) filter was used on volumetric data to generate three types of texture: fine, medium and coarse. This technique, which can be considered as an image filtering process followed by a quantification of texture was used in [15] for classifying colorectal cancer cells. A LoG filter was applied using sigma (σ) values of 0.5 (fine texture type), 1.5 (medium texture type) and 2.5 (coarse texture type). We then split the resulting volumetric texture data using a $10 \times 10 \times 10$ grid, and quantified each sub-volume using three functions, average, entropy and standard deviation, giving a total of 9 texture features per sub-volume.

2.2.3. 3D-DWT

A 3D Discrete Wavelet Transform (3D-DWT) was constructed by first applying a 2D wavelet transform on the rows and columns of the volume, followed by a 1D wavelet transform along the third dimension [16]. Using this approach, 8 sub-volumes of lower resolution were obtained: one approximation sub-volume and 7 sub-volumes of details. While a variety of wavelet types could be used, in this study, we report results obtained with the Daubechies (db2), biorthogonal (bior1), Coiflet (coif1), and Symlet (sym2) wavelets. These wavelet families are among the most commonly used, and typically achieve a good spatial-frequency localization trade off using narrow high-pass and wide low-pass filters. In this work, we quantified the details (high-frequency) sub-volumes using three functions: namely, average, entropy and standard deviation. Thus, each sub-volume obtained by grid splitting is represented by a vector of 21 features.

2.3. Classifier setting and performance metrics

The random forest (RF) algorithm was used to classify subjects from texture features extracted in each sub-volume. This ensemble learning algorithm generates multiple decision trees, each trained from a random sample (with replacement) of training examples, and combines the output of generated trees using a majority vote. A feature bagging process is also used while learning individual trees, in which a random subset of the features is considered for each candidate split [17]. Random forests are particularly useful when, as in our case, the number of features is high compared to the number of training examples. In our experiments, we set the number of decision trees to 100 and the minimum leaf size to 1.

A 10 fold cross-validation approach was used to measure the usefulness of textures, in individual sub-volumes, for classifying subjects as AD or control. The performance of the RF classifier, for each sub-volume, was measured as the mean accuracy (Acc), sensibility (Sens) and specificity (Spec) obtained over the 10 folds. These performance metrics can be defined as

$$\text{Accuracy} = \frac{\text{TP} + \text{TN}}{\text{TP} + \text{FP} + \text{TN} + \text{FN}} \quad (1)$$

$$\text{Sensibility} = \frac{\text{TP}}{\text{TP} + \text{FN}} \quad (2)$$

$$\text{Specificity} = \frac{\text{TN}}{\text{FP} + \text{TN}}, \quad (3)$$

where TP / TN is the number of AD / NC samples (subjects) correctly classified by the model, and FP / FN corresponds to the number of samples incorrectly classified as AD / NC.

An accuracy of 70% was considered as a cut-off for identifying the sub-volumes capable of discriminating between AD and NC subjects.

3. RESULTS AND DISCUSSION

Table 2 gives the mean accuracy, sensitivity and specificity obtained with the three types of texture features in prominent neuroanatomical regions. 3D-GLCM based features achieved an accuracy of 70.16%–74.19%, a sensitivity of 69.35%–75.81%, and a specificity of 66.13%–77.42%, the highest accuracy obtained in the occipito-temporal gyrus. In comparison, LoG based features lead to an accuracy of 70.16%–74.19%, with the highest performance (accuracy of 74.19%, sensitivity of 72.58% and specificity of 75.81%) observed in the uncus region. Moreover, an accuracy of 70.16%–71.77% was obtained for 3D-DWT based features, the highest value found in the pons region using Symlet wavelets. No significant region was found for Coiflet and biorthogonal wavelets (i.e., accuracy less than 70%). Overall, 3D-GLCM and LOG based features resulted in the highest accuracy.

Figure 3 shows the location of discriminative regions found using the three types of textures. We notice that the location of these regions differs between texture types, suggesting that different texture features encode distinct characteristics of AD. Moreover, we observe that most discriminative regions were found using 3D-GLCM and LoG texture features, confirming their advantage over 3D-DWT features. While many of these regions correspond to known results in the literature [11], several brain regions not traditionally linked to AD also showed the ability to discriminate between AD and control subjects: gyrus (left and right) of occipito-temporal, red nucleus, pons, genu of internal capsule, uncus, central sulcus, transverse sinus, and occipital horn of lateral ventricle. Further work is required to fully understand the role of these regions in the progression of AD.

Table 2. Texture features and approximate neuroanatomical regions with classifier accuracy > 70%. Note that regions labels are defined in the axial plane.

Texture	Acc	Sens	Spec	Brain regions
GLCM (156 features)	72.58	72.58	72.58	Thalamus
	70.16	69.35	70.97	Occipito-temporal G. R.
	70.16	72.58	67.74	Insula
	70.97	70.97	70.97	Pre-central G. R.
	71.77	69.35	74.19	Post-central G. R.
	74.19	70.97	77.42	Occipito-temporal G. L.
	70.97	75.81	66.13	Red nucleus
DWT-db2 (24 features)	70.16	74.19	66.13	Genu of corpus callosum
DWT-coif1 (24 features)	< 70	-	-	-
DWT-bior1 (24 features)	< 70	-	-	-
DWT-Sym1 (24 features)	71.77	62.90	80.65	Pons
LoG filter (9 features)	70.97	70.97	70.97	Ginu of int. Capsule
	74.19	72.58	75.81	Uncus
	70.16	66.13	74.19	Postcentral G. R.
	70.16	66.13	74.19	Central sulcus
	70.16	70.97	69.35	Postcentral G. L.
	70.16	74.19	66.13	Transverse Sinus
	70.16	67.74	72.58	Occipital horn of lateral ventricle
* G: gyrus; Sup: superior; Inf: inferior; R: right; L: left; A: axial; C: coronal; S: sagittal; Int: internal				

4. CONCLUSION

This paper proposed a novel approach for detecting and characterizing AD-related brain changes, based on local texture features derived from brain MRI. Texture features are computed from sub-volumes throughout the brain, and automatic classification performance (e.g. accuracy, sensitivity and specificity) is used to identify discriminative, AD-informative (texture type, brain region) combinations. Experiments make use of three texture feature types (3D-GLCM, 3D-DWT and LoG texture features) and the random forest classifier. Our study revealed several (texture type, brain region) combinations capable of classifying between AD and healthy control subjects with high accuracy, and included several brain regions not traditionally linked to AD. These (brain region/texture feature) combinations may thus prove useful as new imaging biomarkers for detecting and characterizing AD. While this study has underlined the importance of texture features for the analysis of neurodegenerative diseases such as AD, further research is required to fully understand the relationship between textures and the underlying neural substrate of AD, both at a microscopic and macroscopic level.

5. REFERENCES

[1] J. R. Petrella, R. E. Coleman, and P. M. Doraiswamy, "Neuroimaging and early diagnosis of Alzheimer dis-

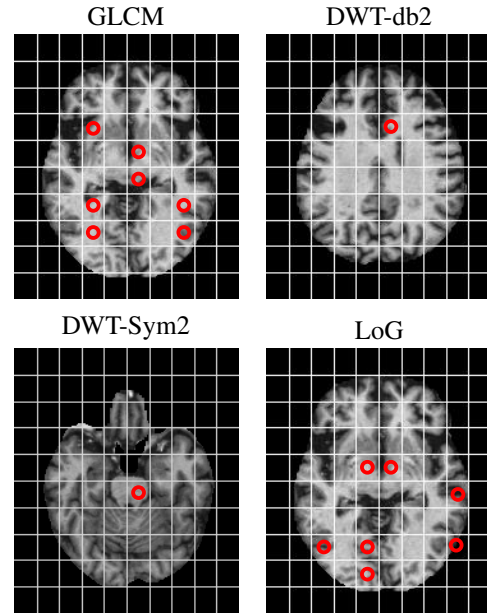


Fig. 3. Location of discriminative brain regions found using different texture features. Images are shown in the axial plane.

ease: a look to the future," *Radiology*, vol. 226, no. 2, pp. 315–336, Feb. 2003.

- [2] Alzheimer's Association, "2013 Alzheimer's disease facts and figures," *Alzheimers Dement. J. Alzheimers Assoc.*, vol. 9, no. 2, pp. 208–245, Mar. 2013.
- [3] D. P. Devanand, G. Pradhaban, X. Liu, A. Khandji, S. De Santi, S. Segal, H. Rusinek, G. H. Pelton, L. S. Honig, R. Mayeux, Y. Stern, M. H. Tabert, and M. J. de Leon, "Hippocampal and entorhinal atrophy in mild cognitive impairment: prediction of Alzheimer disease," *Neurology*, vol. 68, no. 11, pp. 828–836, Mar. 2007.
- [4] R. S. Desikan, H. J. Cabral, C. P. Hess, W. P. Dillon, C. M. Glastonbury, M. W. Weiner, N. J. Schmansky, D. N. Greve, D. H. Salat, R. L. Buckner, B. Fischl, and Alzheimer's Disease Neuroimaging Initiative, "Automated MRI measures identify individuals with mild cognitive impairment and Alzheimer's disease," *Brain*, vol. 132, no. 8, pp. 2048–2057, Aug. 2009.
- [5] S. Farhan, M. A. Fahiem, and H. Tauseef, "An Ensemble-of-Classifiers Based Approach for Early Diagnosis of Alzheimer's Disease: Classification Using Structural Features of Brain Images," *Comput. Math. Methods Med.*, vol. 2014, p. e862307, Sep. 2014.
- [6] E. Gerardin, G. Chételat, M. Chupin, R. Cuingnet, B. Desgranges, H.-S. Kim, M. Niethammer, B. Dubois, S. Lehéricy, L. Garnero, F. Eustache, and O. Colliot, "Multidimensional classification of hippocampal shape fea-

- tures discriminates Alzheimer's disease and mild cognitive impairment from normal aging," *NeuroImage*, vol. 47, no. 4, pp. 1476–1486, Oct. 2009.
- [7] M. Toews, W. Wells, D. L. Collins, and T. Arbel, "Feature-based morphometry: discovering group-related anatomical patterns," *NeuroImage*, vol. 49, no. 3, pp. 2318–2327, Feb. 2010.
- [8] P. A. Freeborough and N. C. Fox, "MR image texture analysis applied to the diagnosis and tracking of Alzheimer's disease," *IEEE Trans. Med. Imaging*, vol. 17, no. 3, pp. 475–479, Jun. 1998.
- [9] J. Rajeesh, "Discrimination of Alzheimer's disease using hippocampus texture features from MRI," *Asian Biomed.*, vol. 6, no. 1, Jan. 2012.
- [10] N. Aggarwal, B. Rana, and R. K. Agrawal, "3D discrete wavelet transform for computer aided diagnosis of Alzheimer's disease using T1-weighted brain MRI," *Int. J. Imaging Syst. Technol.*, vol. 25, no. 2, pp. 179–190, Jun. 2015.
- [11] M. Li, K. Oishi, X. He, Y. Qin, F. Gao, S. Mori, and for the Alzheimer's Disease Neuroimaging Initiative, "An Efficient Approach for Differentiating Alzheimer's Disease from Normal Elderly Based on Multicenter MRI Using Gray-Level Invariant Features," *PLoS ONE*, vol. 9, no. 8, p. e105563, aot 2014.
- [12] R. Maani, Y. H. Yang, and S. Kalra, "Voxel-Based Texture Analysis of the Brain," *PLoS ONE*, vol. 10, no. 3, Mar. 2015.
- [13] D. S. Marcus, T. H. Wang, J. Parker, J. G. Csernansky, J. C. Morris, and R. L. Buckner, "Open Access Series of Imaging Studies (OASIS): cross-sectional MRI data in young, middle aged, nondemented, and demented older adults," *J. Cogn. Neurosci.*, vol. 19, no. 9, pp. 1498–1507, Sep. 2007.
- [14] R. M. Haralick, K. Shanmugam, and I. Dinstein, "Textural Features for Image Classification," *IEEE Trans. Syst. Man Cybern.*, vol. SMC-3, no. 6, pp. 610–621, Nov. 1973.
- [15] Ahmad Chaddad, Ahmed Bouridane, and Camel Tanougast, "Continuum Analysis of Colorectal Cancer Using Texture Feature Extraction," *45th International Conference on Computers & Industrial Engineering*, Metz, France, 2015, p. in press.
- [16] Z. Chen and R. Ning, "Breast volume denoising and noise characterization by 3D wavelet transform," *Comput. Med. Imaging Graph. Off. J. Comput. Med. Imaging Soc.*, vol. 28, no. 5, pp. 235–246, Jul. 2004.
- [17] L. Breiman, "Random forests". *Machine learning*, vol. 45, no. 1, pp. 5–32, 2001.